Atmos. Chem. Phys. Discuss., 10, 1719–1754, 2010
www.atmos-chem-phys-discuss.net/10/1719/2010/

Atmospheric Chemistry and Physics Discussions

This discussion paper is/has been under review for the journal Atmospheric Chemistry and Physics (ACP). Please refer to the corresponding final paper in ACP if available.

Ozone reservoir layers in a coastal environment – a case study in Southern Taiwan

C.-H. Lin[1], Y.-L. Wu[2], and C.-H. Lai[1]

[1]Department of Environmental Engineering and Science, Fooyin University, Kaohsiung, Taiwan
[2]Department of Environmental Engineering, National Cheng-Kung University, Tainan, Taiwan

Received: 4 October 2009 – Accepted: 14 December 2009 – Published: 21 January 2010

Correspondence to: C.-H. Lin (chlin@mail.fy.edu.tw)

Published by Copernicus Publications on behalf of the European Geosciences Union.

Abstract

The air layer between the nocturnal boundary layer and the top of the daily mixing layer in an ozone-polluted area is known to serve as an ozone reservoir since the ozone that is produced in the previous daytime mixing layer can be well preserved throughout the night in the air layer. Ozone reservoir layers are capable of enhancing surface ozone accumulation on the following day. However, our knowledge of the characteristics of ozone reservoir layers and their effects on the daily ozone accumulations is limited. In this work, ozone reservoir layers were experimentally investigated at a coastal, near-mountain site in Southern Taiwan, 30 km away from the coastlines. Tethered ozone soundings were performed to obtain vertical profiles of ozone and meteorological variables during a four-day ozone episode in November 2006. Observation-based methods are adopted to evaluate the influences of the ozone reservoir layers on the surface ozone accumulation during the four-day ozone episode. Ozone reservoir layers were found to develop every evening with a depth of 1200–1400 m. Ozone concentrations within the reservoir layers reached over 140 parts per billion (ppb). From each evening to midnight, the size of the ozone reservoir layer and the ozone concentration inside dramatically changed. As a result, a concentrated, elevated ozone reservoir layer formed with a depth of 400 m at 800–1200 m every midnight. For the rest of each night, the elevated ozone reservoir layer gradually descended until it reached 500–900 m in the next morning. Local circulations and nocturnal subsidence are responsible for the observed evolution. The ozone concentration at the study site was maximal at 15:00–17:00 LT daily because of the addition of the daily produced ozone on the preceding day. Hourly downward mixing ozone concentrations due to the ozone reservoir layers can be as high as 35–45 ppb/h in the late morning. The contribution of the ozone carried over from the preceding day can be 75–85 ppb, which contributes over 50% to the daily ozone pollution as compared with ozone produced on the study day.

ACPD

10, 1719–1754, 2010

1 Introduction

Understanding the processes that drive the ozone accumulations in the boundary layer is important because of the adverse impacts of ozone on human health, plants and global warming (Fuhrer, 2003). Surface ozone levels can rise after sunrise from single digits or zero parts per billion (ppb) to more than 120 ppb in the afternoon (National Research Council, 1991). Processes attributable to the accumulation of ozone can be easily revealed from a photochemical trajectory box model (Evans et al., 2000),

$$\frac{dC}{dt} = \frac{\partial C}{\partial t} + \left(U\frac{\partial C}{\partial x} + V\frac{\partial C}{\partial y}\right) = (P - LC) - C\frac{v_d}{h} + (C_r - C)\frac{1}{h}\frac{dh}{dt} \quad (1)$$

I II III IV V VI

where C is the ozone concentration within a considered travelling air box whose vertical height is consistent with a variant mixing height, h; U and V represent the averaged wind speeds in the x and y directions within the mixing layer; P and LC represent the rates of photochemical production and loss; v_d is the dry deposition velocity; and C_r is the ozone concentrations above the mixing layer. Notably, C_r can be regarded as the ozone concentration in an ozone reservoir layer because most daily photochemically produced ozone is within the mixing layer. Terms in Eq. (1) represent (1) I, the observed, total ozone variation rate within the considered travelling air box; (2) II, the observed, total ozone variation rate at a specific location (x, y) based on an Eulerian approach; (3) III, the ozone variation rate due to horizontal advection; (4) IV, the ozone variation rate due to net photochemical production; (5) V, the ozone variation rate due to dry deposition; and (6) VI, the ozone variation rate due to net vertical entrainment. Clearly, a positive ozone variation rate, as observed at a specific location in the daytime mixing layer, (II), is probably caused by three processes – the horizontal advection (III), net photochemical production (IV), and net vertical entrainment (VI).

Emission-based air quality models can be used to calculate explicitly the contributions of the three processes to the daytime ozone accumulation at a location of interest

ACPD
10, 1719–1754, 2010

(Russell and Dennis, 2000). However, the calculated contributions are frequently associated with significant uncertainties, particularly due to the difficulties in acquiring accurate emission inventories (Placet et al., 2000) and in effectively simulating boundary layer dynamics (Dabberdt et al., 2004). An alternative method, which couples the measured ozone and its precursors and the dynamics of the boundary layer, is known an observation-based method (Trainer et al., 2000; Cardelino and Chameides, 2000), and can complement emission-based models. Observation-based methods have been extensively developed in the past decade to evaluate photochemical production rates (Trainer et al., 1991, 2000; Cantrell et al., 1996; Spirig et al., 2002; Kleinman, 1986; Cardelino and Chameides, 2000; Gerasopoulos et al., 2006; Frost et al., 1998; Baumann et al., 2000; Shiu et al., 2007). However, an observation-based method has not yet been to analyze the contribution of horizontal advection or vertical entrainment. This shortcoming is partially explained by the difficulty in making vertical measurements of ozone and meteorological variables simultaneously with a high time resolution. This work develops an observation-based method and applies it to evaluate the contribution of the ozone due to vertical entrainments to daily ozone pollution in a field study.

Several investigations have explained the formation of an ozone reservoir layer and its possible enhancement of the surface ozone concentration on the following day (Neu et al., 1994; Stull, 1998; Zhang and Rao, 1999). Figure 1 summarizes these explanations. However, different structures of ozone reservoir layers from the proposed model (Fig. 1) can be expected. For example, nighttime transport can distort ozone reservoir layers. Several field studies have demonstrated the importance of complicated nighttime transport aloft (Banta et al., 1998; Hidy, 2000). In addition to possibly elevated NO titration, nocturnal chemistry, dominated by the nitrate radical, NO_3, can also cause the loss of ozone, $NO_2+O_3 \rightarrow NO_3+O_2$ (Brown et al., 2003; Stutz et al., 2004). Our knowledge of the characteristics of ozone reservoir layers and their effects on the daily ozone accumulations is limited.

In this work, four days of complete diurnal and nocturnal variations of vertical ozone and meteorological profiles are obtained from tethered ozone soundings that were

ACPD
10, 1719–1754, 2010

intensively performed during a field study during November 2006 in Southern Taiwan. The characteristics of the observed ozone reservoir layers, their driving processes and their effects on daily ozone accumulations are investigated and discussed.

2 Experimental setup

2.1 Site description

Figure 2 shows location of the study site (22.826° N, 120.529° E, 10 m a.s.l.) and its surroundings. It is a coastal site near mountains, in an agricultural area, 30 km from the western coastline and 7.5 km from the eastern edge of the Central Mountain Ranges (CMR). Major sources are located at least 30 km away from the study site, including vehicles and industrial parks in and around the industrial Kaohsiung City and Shingda (SD) coal-fire power plant (4300 MW) on the western coastline. Pollutants from sources in central or Northern Taiwan can also be transported to the study site when ambient flows are northerly. Although the main sources are located 30 km away, ozone pollution in the study area is unexpectedly high. For example, in 2006, the Meilung (ML) air station, 7 km north of the study site, recorded 29 days on which Taiwan's 1-h ozone standard of 120 ppb was violated (Taiwan EPA, 2007).

2.2 Measurements

A tethered sounding system was installed at the study site to measure vertical profiles of ozone and other meteorological variables. Our earlier work adopted similar systems (Lin et al., 2004). Tethered soundings were performed daily from 29 October to 12 November 2006 and intensively performed during a high-ozone period, 8–11 November. On days of high ozone concentration, soundings were preformed every 2–4 h, typically reaching altitudes of 1400–1600 m when the meteorological conditions permitted. The system consisted of a helium-filled balloon with a diameter

ACPD
10, 1719–1754, 2010

of 3 m, attached to an electric winch via a 2 km-long Kevlar line. Commercial tethered ozonesonde TTO111 (Vaisala, Finland) and meteorological radiosondes TTS111 (Vaisala, Finland) were used to measure vertical ozone and meteorological variables (pressure, temperature, relative humidity, wind speed and wind direction) simultaneously. The sondes were tethered on the tethered line, 15 m below the balloon. The ascent and descent of the balloon were controlled using the electric winch. Both ascending and descending profiles were acquired in each sounding. The ozonesonde sensor was an SPC (Science Pump Corporation, USA) model 6A ECC (Electrochemical Concentration Cell). A buffered 1% KI solution was used in the cathode half-cell and a saturated KI solution was used in the anode half-cell, as suggested by Komhyr (1969) and Komhyr et al. (1995). Before each sounding was conducted, the measurements of the meteorological radiosonde were checked with those at an on-site MAWS 201 surface weather station (Vaisala, Finland), which was installed during the field study. Zero and one-point calibrations of the ECC ozonesondes were also performed. The accuracy of the ECC ozonesonde was within 6% in the lower troposphere (Komhyr et al. 1995).

2.3 Synoptic weather and surface ozone levels in Taiwan during 8–11 November

During 8–11 November, the synoptic weather in Taiwan was dominated by a continental anticyclone emanating from mainland China, which was moving eastward (Fig. 3). This synoptic weather pattern along with serious ozone pollution is typical in Western Taiwan (Cheng et al., 2001; Chen et al., 2003; Lin et al., 2007). During this period, Taiwan was at the outer edge of the high-pressure system. The ambient flows toward Taiwan became northeasterly and were blocked by the CMR. Since the solar radiations was sufficiently intense and the ventilation was poor, ozone concentrations quickly increased on 8 November (Fig. 4), and increased further on 9–10 November as the anticyclone moved further eastward and the blocking effect became more important.

On 11 November, a weak front approached Taiwan, the ozone pollution in Northern and Central Taiwan significantly decreased but in Southern Taiwan, the ozone

ACPD
10, 1719–1754, 2010

concentrations reached the highest levels within the four-day study period. Figure 4 plots the ozone distributions and wind fields throughout Taiwan in the afternoons from 7 to 12 November, interpolated from the measurements made at the air stations of Taiwan Air Quality Monitoring Network (TAQMN). From 8 to 11 November, the daily numbers of air stations of the TAQMN that reported violation of the 1-h ozone standard of 120 ppb were 15, 23, 24 and 6. This ozone episode in Taiwan was the most important in 2006. The ozone pollution days are clearly associated with relatively light and landward winds in the afternoon (Fig. 4), suggesting poor ventilations and the development of local circulations. Daily maximum hourly ozone concentrations reached as low as 40 ppb on 8–10 November in the upwind northeastern and eastern parts of Taiwan (Fig. 4), suggesting that the ozone episode was not attributable to long-range transport, such as from mainland China (Akimoto et al., 1996; Junker et al., 2009).

3 Results and discussion

3.1 Daily evolution of ozone reservoir layers

Figure 5a plots the time-height relationship of each the ozone soundings and the corresponding number of the soundings from 8 to 11 November. A total of 28 soundings were performed over the four days. Figure 5b presents some of the ozone profiles obtained during the soundings, to reveal daily cycles in vertical ozone distributions from the afternoon to the following noon. These profiles are the averages of ascending and descending measurements. Additionally, hourly vertical ozone distributions are obtained by linearly interpolating all of the measured ozone profiles, enabling continuous variations of vertical ozone distributions to be clearly observed (Fig. 5c). No distinct elevated ozone layer was observed on the morning of 8 November (Fig. 5c) because of light ozone pollution present in the previous afternoon (Fig. 4). Moreover, the evolution of vertical ozone distribution after noon on the last day, 11 November, differed from the previous on the three days. This difference resulted from changes in the wind fields on the morning of 11 November (Fig. 6a).

ACPD
10, 1719–1754, 2010

The ozone reservoir layer is defined herein as the air in which the ozone concentrations apparently exceed the regional background values. Moreover, the ozone reservoir layers are present from evening to the next morning at the altitudes below those of the daily maximum mixing layers. The background ozone levels in the free atmosphere are 60–70 ppb, as determined from some soundings reaching relatively high altitudes. Therefore, the ozone reservoir layers can be identified as those with ozone concentrations over 80 ppb from evening to the next morning. Based on this principle, the daily evolutions of the ozone reservoir layers were quite similar among the three nights from the evening of 8 November to the morning of 11 November (Fig. 5c). The evolution of the ozone reservoir layers on the three nights can be simply divided into two stages – a developing stage (I) and a stable, descending stage (II) (Fig. 5c). Stage I began at 15:00–17:00 LT, lasted for 5–8 h, and ended at 22:00–23:00 LT. Stage II began at mid-night, lasted for 8–10 h, and ended at 08:00–10:00 LT.

Before the beginning of stage I, at 12:00–15:00 LT, vertical ozone concentrations at 0–1300 m were uniformly distributed, as indicated in the ozone profiles nos. 3, 11, and 18 in Fig. 5b and c. The uniformity of the ozone concentration resulted from convective mixings every afternoon. At 15:00–17:00 LT daily, surface ozone concentrations reached their daily maximums. Thereafter, a residual layer (RL)-like ozone layer formed. The formation of the RL-like ozone layer marked the beginning of stage I of the daily evolution of the ozone reservoir layer (Fig. 5c). In the first 2–3 h of stage I, ozone concentration above the ground increased continuously, particularly from 400 to 1200 m, as indicated in the ozone profiles nos. 4, 13 and 20 in Fig. 5b. Thereafter, ozone concentrations at 200–800 m began to significantly decrease until midnight (Fig. 5c). However, the ozone concentrations at 800–1200 m were roughly invariant in the last 3–4 h of stage I. By midnight, the variations in the vertical ozone distribution became small and a concentrated, elevated ozone reservoir layer formed at 800–1200 m, as indicated in the ozone profiles nos. 5, 14 and 21 in Fig. 5b and c. Interestingly, an ozone-depleted air layer was observed at 500–700 m at midnight between 9 and 10 November, as indicated in the ozone profiles nos. 14 and 15 in

ACPD
10, 1719–1754, 2010

Fig. 5b and c. The possible cause of the elevated ozone depletion will be discussed later.

In stage II of the daily evolution of the ozone reservoir layers, the vertical ozone distributions were stable but the concentrated, elevated ozone layer descended by about 250 m from 950 m at midnight to around 700 m at 9:00 LT in the next morning, as indicated in the ozone profiles nos. 9, 17 and 24 in Fig. 5b and c. Finally, the elevated ozone layer merged into the developing mixing layer at 10:00–12:00 LT (Fig. 5c). Notably, the similarity of the evolution of the daily ozone reservoir layers suggests that the evolution was driven by some regular, daily processes. Furthermore, the observed evolution (Fig. 5b and c) differed from that in the generally accepted model, as presented in Fig. 1. The differences were probably caused by the fact that the evolution in this study was observed in the coastal environment whereas the general model (Fig. 1) was constructed based on the experiments conducted inland on a relatively flat continent (Neu et al., 1994; Stull, 1998; Zhang and Rao, 1999). Nighttime transport is expected to be more complicated in a coastal environment than in a continental one.

3.2 Processes driving the evolution of coastal ozone reservoir layers

Figure 6 shows the wind, potential temperature, water mixing ratio, and daytime mixing layer superimposing on ozone contours. Like ozone concentration (Fig. 5c), these variables are obtained from linear interpolations of the sounding profiles of these variables. The top of a daytime mixing layer was identified at the altitude where the gradients of potential temperature and water mixing ratio were strong, as suggested by Stull (1988). Figures 7 and 8 show some sounding profiles from the evening of 9 November to the next morning, to help explain the factors that drive the evolution of the observed ozone reservoir layers. Backward air trajectories, starting from the study site, were calculated every four hours, at the altitudes of 200, 400, 600, 800, 1000 and 1200 m to identify the origins of the different air masses that arrived at the study site at different altitudes and times. The calculations of the trajectories are based on the hourly vertical wind distributions (Fig. 6a). Banta et al. (1998) employed a similar approach to analyze the

city plume transport in Nashville, Tennessee. Figure 9 plots the calculated trajectories at 18:00 and 22:00 LT on 9 November, and at 02:00 and 06:00 LT on the next morning to demonstrate typical origins of the air masses at different altitudes in the ozone reservoir layers.

Firstly, the formation of the ozone reservoir layers was found to link to the arrivals of cooler marine masses at 15:00–17:00 LT daily. Evidence for this linkage includes the observations of an afternoon wind circulation (Fig. 6a), a rapid decrease in the mixed layer depth (Fig. 6), a decrease in potential temperature (Fig. 6b), and an increase in the water mixing ratio (Fig. 6c) during the period of formation on each of the four study days. The afternoon circulations included transitional layers that were centered around 800 m (Fig. 6a). Westerly onshore and easterly offshore winds prevailed below and above the transitional layer; they exhibited the behaviors of sea-breeze circulations. Wind directions changed around 800 m, and a rapid decrease in potential temperature and an increase in water mixing ratio, respectively, were clearly observed in the evening sounding of 9 November (Fig. 7a). The decrease in potential temperature and increase in water mixing ratio in Figs. 6b, c and 7a can be explained by the arrivals of cooler, moisture-rich marine air masses. The rapid daily decrease in the mixing layer in the afternoon (Fig. 6) resulted from the formation of a stable layer when a cooler marine air mass invaded the bottom part of a warmer mixing layer in the afternoon. The observed RL-like ozone reservoir layer at this time was the residual of the afternoon mixing layer. Notably, the depth of landward breeze reached as high as 800 m (Fig. 6a), but only the bottom part below 200 m was initially identified as marine air mass with a relatively low potential temperature and high water mixing ratio. Lu and Turco (1994) simulated a similar stabilization of the boundary layer in the evening by an invasion of cool, marine air mass into an inland, deepened and warmer air mass, in a study of the transport of air pollutants in Los Angels Air Basin.

ACPD
10, 1719–1754, 2010

Secondly, the nature of initially increasing and then decreasing in ozone concentration in the lower part of the daily ozone reservoir layer below 800 m in stage I, probably resulted from the arrivals of more marine air masses at the study site. Notably, the beginning and end of the evolution of ozone reservoir layers in stage I were consistent with those of the sea-breeze return flow above 800 m. This consistence suggests that the evolution of the ozone reservoir layers in stage I was related to the sea-breeze circulation. This circulation can also be a combination of a sea breeze, a mountain flow and their return flows. The combination of a sea breeze and a mountain flow is typical in a coastal mountain region (McKendry and Lundgren, 2000; Whiteman et al., 2000). The initially arriving marine air masses were more polluted than those that arrived later because they came from near the coastline where important sources are located. This fact explains why daily surface ozone concentrations were maximal roughly when marine air mass initially arrived at the study site (Fig. 5c). The continuous increase in ozone concentration at 300–800 m in the first 2–3 h of stage I is explained by the later arrivals of polluted coastal air masses at higher altitudes. Notably, the speed of the sea-breeze flow peaked at 150 m and then decreased as the altitude increased (Figs. 6a and 7a). Therefore, polluted near-coast air masses at higher altitudes were expected to arrive later than those at lower altitudes. After the near-coast, polluted air masses, subsequently arriving marine air masses were less polluted, because they came from a more remote, less polluted area over the sea. This fact explains the subsequent, rapid decrease in ozone concentration in the lower parts of the ozone reservoir layer toward the end of stage I. The continuous arrival of marine air masses in stage I was evidenced by the continuous decease in potential temperature and increase in water mixing ratio (Fig. 6b and c). Backward trajectories analysis also indicated that more marine air masses arrived at the study site in stage I as the night progressed. For example, more air masses came from the sea area at 22:00 LT on 9 November (Fig. 9b) than those at 18:00 LT (Fig. 9a). The ozone concentrations at 800–1200 m remained invariant because they were polluted, return inland flows, and were initially located within the convective mixing layer (Fig. 6).

ACPD
10, 1719–1754, 2010

Notably, the elevated plumes emitted from large sources in the coastal area may have been accompanied by the marine air masses and transported to the study site when a sea-breeze circulation prevailed. As mentioned in Sect. 3.1, elevated ozone depletion at 500–700 m was found at night between 9 and 10 November (Fig. 5b and c). Figure 8a depicts one such elevated ozone depletion. Backward trajectories at 22:00 LT on 9 November and 02:00 LT on 10 November (Fig. 9b and c) reveal that air masses at several altitudes had previously passed over the coastal, SD power plant, suggesting that the observed ozone depletion resulted from the NO titration within the SD plume, $NO+O_3 \rightarrow NO_2+O_2$.

After midnight, sea-breeze circulation stopped. No more marine air mass then arrived. Hence, the decrease in the ozone concentration in the lower parts of the ozone reservoir layers ceased. The previously easterly, return flows of the circulations were then replaced with northerly ambient winds (Fig. 6a). However, the direction of the flow changed with altitude. Northeasterly flows typically dominated below 300 m. These were downwardly sloping land breezes, triggered by surface cooling. The flows above the land flows at 400–1000 m were northwesterly, and probably the counterparts of the land breezes. The backward trajectories at 06:00 LT on 10 November (Fig. 9d) clearly revealed the variation in the flow direction with altitude in stage II. The trajectories also suggested that the elevated, concentrated ozone reservoir layer in stage II came from a relatively near-coastal area. The descending in the altitudes of the daily ozone reservoir layer in stage II was likely the result of atmospheric subsidence due to surface cooling (Fig. 3). This process is typical in coastal areas (Simpson, 1994).

During the experiment, the synoptic weather was dominated by a high-pressure system (Fig. 2), probably further enhancing the observed strong subsidence. Nighttime subsidence was revealed by the slight increase in potential temperature and a decrease in the water mixing ratio above 500 m in stage II (Fig. 6b and c). However, the transport of air aloft may also mask the subsidence of the elevated ozone reservoir layers. As mentioned above, the air masses at 500–1000 m came from areas relatively close to the coast. Notably, during the period of prevailing sea-breeze circulation in

ACPD
10, 1719–1754, 2010

stage I, the area aloft near the coast served as a subsidence area. As a result, the elevated ozone layers were relatively low in the near-coast areas. When these lower-level ozone layers were transported to the relatively inland study site in stage II, they may have masked the subsidence occurring at the study site.

Figure 10 shows the conceptual model to summarize the processes that may drive the evolution of the observed coastal ozone reservoir layers. The proposed coastal model and the generally accepted, continental one, as shown in Fig. 1, have the following differences.

1. In the coastal model, an ozone reservoir layer is formed due to the invasion of a cool, marine air mass into a relatively warm mixing layer in the evening but in the continental model, an ozone reservoir layer is formed by surface cooling after sunset.

2. From evening to midnight, the lower part of the ozone reservoir layer in the coastal model, roughly below 800 m, becomes less polluted because of the arrivals of remote, less polluted marine air masses. This evolution does not occur in the continental model.

3. From midnight to next morning, the ozone reservoir layer in the coastal model significantly descends because of nocturnal subsidence. The subsidence is expected to be stronger in the coastal model than that in the continental model.

4. Large increases in surface ozone concentration in the morning due to the downward mixing of the ozone from the ozone reservoir layers probably occur 1–2 h later in a coastal environment than that in a continental one because the ozone reservoir layer is higher in the former than in the latter. Section 3.4 will elucidate this feature.

The air flow at 400–800 m frequently blew landward. For example, in the daytime, the flow at 0–800 m was a landward sea breeze and at night, the flow at 400–1000 was a landward, returning, land breeze. Therefore, the plumes emitted from large coastal

point sources, such as the SD power plant (Fig. 8c), can be transported inland both day and night. This previously unnoticed feature may have played an important role in the serious ozone pollution of the inland study area. This effect must be further investigated.

3.3 Downward mixing ozone and the ozone from the preceding day

Ozone that was observed in the early-morning ozone reservoir layers (Fig. 5c) was carried over from the preceding day. This ozone has enhanced surface ozone concentrations by downward mixing while the daytime mixing layers were developing during the experiment. This feature was captured in the daily morning soundings during the field study. Figure 8b depicts such an example. Notably, the net vertical entrainment term consists of two sub-terms (Evans et al., 2000). The first sub-term,

$$C_{\mathrm{r}} \frac{1}{h} \frac{dh}{dt}, \tag{2}$$

is the increase rate in surface ozone concentration due to downward mixing of the ozone from the ozone reservoir layer into the growing mixing layer. The second sub-term,

$$-C \frac{1}{h} \frac{dh}{dt}, \tag{3}$$

is the decrease rate in surface ozone concentration due to the expansion or dilution of the ozone in the growing mixing layer. Apparently, the net vertical entrainment term in Eq. (1) is positive if the increase rate due to downward mixing is larger than the decreased rate due to dilution and vice versa. In the following, the interpolated hourly ozone profiles and mixing layer depths (Fig. 6) are coupled with finite difference methods to estimate different contributions to the variation rates in surface ozone concentration from downward mixing process and the net vertical entrainment term;

$$\Delta C_n = C(t_n) - C(t_{n-1}) \tag{4}$$

ACPD
10, 1719–1754, 2010

$$\Delta D_n = C_r(t_{n-1}) \frac{h(t_n) - h(t_{n-1})}{h(t_n)} \quad (5)$$

$$\Delta E_n = \left[C_r(t_{n-1}) - C(t_{n-1})\right] \frac{h(t_n) - h(t_{n-1})}{h(t_n)} \quad (6)$$

where ΔC_n is the total increase in surface ozone concentration in the n-th hour at the study site; ΔD_n and ΔE_n are the contributions to ΔC_n from downward mixing process and net vertical entrainment term in the n-th hour, respectively; $C(t_n)$ and $C(t_{n-1})$ are the averaged ozone concentrations in the mixing layer at times t_n and t_{n-1}, respectively; $C_r(t_{n-1})$ is the ozone concentration in the reservoir layer at time t_{n-1}, obtained by averaging ozone profile at time t_{n-1} from an altitude of $h(t_{n-1})$ to $h(t_n)$; and $h(t_{n-1})$ and $h(t_n)$ are the mixing heights at times t_{n-1} and t_n, respectively. Notably, the contributions of the ozone from downward mixing process and net vertical entrainment term become zero when the mixing layers stop growing or become even lower, typically in the daily afternoon.

The ozone in a daily mixing layer comprises ozone carried over from the preceding day and produced on the current day. Determining the contribution of the ozone from the preceding day and that of the current day is important for developing an effective ozone control strategy. The contribution of the ozone from the preceding day is estimated by integrating all of the hourly contributions of the ozone from downward mixing process, while considering the ozone decrease due to dilution in each subsequent hour,

$$S_n = \frac{S_{n-1} h(t_{n-1})}{h(t_n)} + \Delta D_n \quad (7)$$

where S_n and S_{n-1} are the contributions of the ozone from the preceding day to $C(t_n)$ and $C(t_{n-1})$, respectively, at times t_n and t_{n-1}. Similarly, the contributions remain the same when the mixing layers stop growing or become even lower. Chemical reaction and dry deposition can affect the contribution of the ozone from the preceding day. The

ACPD
10, 1719–1754, 2010

influence from chemical reaction can be positive or negative and will not be considered here. The influences due to dry deposition is estimated by,

$$SD_n = \left[\frac{SD_{n-1}h(t_{n-1})}{h(t_n)} + \Delta D_n\right] - \left[\frac{SD_{n-1}h(t_{n-1})}{h(t_n)} + \Delta D_n\right]\frac{v_d}{0.5\left[h(t_n)+h(t_{n-1})\right]} \quad (8)$$

where SD_n and SD_{n-1} are the contribution of the ozone from the preceding day at the n-th and $(n-1)$-th hours, determined by considering dry depositions losses. Notably, the second term on the right-hand side of Eq. (8) is a finite difference form of the exact dry deposition term, V, in Eq. (1). In Eq. (8), the dry deposition velocities are linearly increasing from 0.2 cm/s at 07:00 LT to 0.4 cm/s at 12:00 LT and linearly decreasing from 0.4 cm/s at 13:00 LT to 0.2 cm/s at 18:00 LT. The used velocities are typical in an agricultural area during the fall season (Wesely and Hicks, 2000).

The contribution of the ozone produced on the current day is estimated by,

$$PD_n = C(t_n) - SD_n \quad (9)$$

where PD_n is the contribution of the ozone produced on the current day to $C(t_n)$ at the n-th hour, obtained simply by subtracting the contribution of the ozone from preceding day from the average concentration of ozone in the mixing layer at the n-th hour.

Figure 11 plots results calculated using the Eqs. (4)–(9) and hourly ozone concentrations within the mixing layers from 8 to 11 November. Notably, the contribution of the ozone from downward mixing and that of the ozone from net entrainment term in hours 6 and 7 are zero because no convective mixing layer was found at those hours. Apparently, on most days, the hourly downward mixing ozone concentrations are larger than the hourly ozone increases in the mixing layer; the latter are also larger than the net entrainment ozone concentrations. From daily sunrise to 13:00–14:00 LT, the hourly variations of the downward mixing ozone concentration, the increase in the ozone concentration in the mixing layer, and the net entrainment ozone contribution are consistent with each other. These features suggest that the contribution of downward mixing ozone dominates the variation in hourly ozone concentration in the mixing layer

ACPD
10, 1719–1754, 2010

and the contribution of the hourly net entrainment ozone from sunrises to daily 13:00–14:00 LT. The daily maximum hourly downward mixing ozone concentrations are 28, 45, 35 and 46 ppb on the four study days from 8 to 11 November. The value on the first day, 28 ppb, is low because no concentrated ozone reservoir layer was present on the morning.

Notably, two peaks were found in the hourly variation of the downward mixing ozone concentration, the net entrainment ozone concentration, and the increase in the ozone concentration in the mixing layer in the mornings, at around 8–9 and 11:00–12:00 LT daily. The first daily peaks were related to the time of the surface temperature inversion breaking. During this period, ozone gradients near the ground became very large, because of losses by dry deposition since the previous evenings. The growing rates of mixing layers were also high in the period. Both of these two factors increase the net entrainment ozone contribution, Eq. (6), and were responsible for the first daily peaks. The second daily peaks were consistent with the time of daily penetration of the growing mixing layers by the concentrated ozone reservoir layers at 500–900 m (Fig. 6). Therefore, the second daily peaks resulted from the downward mixing of the ozone from the daily concentrated ozone reservoir layers. The lack of a concentrated ozone reservoir layer in the morning of the first day reasonably explains the absence of the second peak of the net entrainment contribution on the first day (Fig. 10a). Figure 11 also indicates that daily hourly downward mixing ozone concentrations become small or even become zero after 13:00–15:00 LT daily. However the ozone concentrations in the afternoon mixing layer still increased after 13:00–15:00 LT daily, suggesting that the daily produced ozone dominated the increase in surface ozone concentration thereafter.

The contribution of the ozone from the preceding day to the ozone concentration within the mixing layer was maximal at 13:00–15:00 LT daily. The maximum values, when dry depositions losses are not considered, are 60, 74, 77 and 86 ppb on the four study days. When dry depositions losses are accounted for, the daily maximum values are reduced by only 4–5 ppb, suggesting that dry deposition only has a small influence.

ACPD
10, 1719–1754, 2010

The maximum value of 60 ppb on the first day exceeds the expected value because no concentrated ozone reservoir layer was observed on that morning (Fig. 6a). The value is unexpectedly high possibly because of transport or photochemical production occurring above the mixing layer in the mid-morning of the first day. To check this possibility, the daily hourly ozone profiles used in Eq. (6) are replaced with daily ozone profiles at 06:00 LT. Then, the hourly downward mixing ozone concentrations and the ozone concentrations from the preceding day for each of the four study days are recalculated. Clearly, the daily ozone profiles at 06:00 LT are not influenced by the daily photochemical production because of a lack of solar radiation at the time. Therefore, the recalculated contribution of the ozone from the preceding day can avoid the addition of ozone concentration photochemically produced above the mixing layer. Figure 11 presents the recalculated ozone concentrations from the preceding days, SD_6 based on the daily 06:00 LT ozone profiles. Surprisingly, these concentrations differ by only 2–3 ppb from those on the last three days, calculated from Eq. (8), suggesting that photochemical production or elevated transport above the mixing layers is unimportant in the last three days. However, the value on the first day, 48 ppb, was 12 ppb lower than that calculated from Eq. (8), 60 ppb. The difference is probably caused by the relatively strong activity of the photochemical reaction occurring above the mixing layer on the morning of the first day. The ozone precursors should be relatively abundant on the first morning because numerous precursors may have been carried from the preceding day due to a lack of photochemical activities on the preceding day. Notably, the recalculated ozone concentrations increase by almost 40 ppb over the four study days. This increase equals to the increase in the daily maximum ozone concentrations within the daily mixing layers over the four study days. The daily maximum ozone concentration within the mixing layers was 103 ppb on the first day, increasing to 141 ppb on the fourth day (Fig. 11). The same order of magnitude of the increases suggests that the increase in the maximum ozone concentration in the mixing layer over the four days was caused by the increase in the amount of the ozone that was carried over from the preceding day.

ACPD
10, 1719–1754, 2010

The contribution of the ozone produced on the current day to the ozone concentration in the mixing layer was maximal at 15:00–17:00 LT daily. They were 44, 43, 46 and 58 ppb for the four study days (Fig. 11). Interestingly, the contribution on the last day is 12–15 ppb higher than those on the first three days. Notably, the ambient winds became southerly on the morning of the last day. Analysis of backward trajectories (not shown) indicates that the air masses that arrived at the study site in the afternoon of the fourth day had previously passed over the highly emitting areas around the Kaohsiung City (Fig. 2). Additional pollutants must have entered into the arriving air masses as they passed over the highly emitting area, resulting in the relatively high concentration of the ozone produced on the last day. The concentrations of daily produced ozone reached their daily maximums at 15:00–17:00 LT, and not around noon, when photochemical activity was expected to be the strongest under strong solar radiation. This result follows from the fact that most of the produced ozone daily was produced within the coastally originating polluted air masses. The ozone may have been produced before each air mass arrived at the study site at 15:00–17:00 LT daily. The percentage contributions of the ozone from the preceding days to the daily maximum ozone concentrations in the mixing layers were 58, 61, 62 and 59% on the four study days. Those of the ozone produced on each of the four study days were 42, 39, 38 and 41%. On average, the percentage contribution of the ozone from the preceding day and that of the ozone produced on the current day were 60 and 40%, respectively. Notably, the near-coastal relatively polluted air masses affected the study site on each of the four study days. Therefore, the study site is representative of polluted, Southern Taiwan. The downward mixing ozone was generally expected to dominate the maximum surface ozone level in remote, clean areas whereas the daily produced ozone was expected to dominate the maximum level in polluted areas, particularly on days of ozone episodes. However, the current results suggest that even in a highly polluted area, such as Southern Taiwan, on an ozone episode day, the downward mixing ozone or the ozone from the preceding day may still contribute 50% more to daily ozone pollution than the ozone produced on the day of interest. More attention should, therefore,

ACPD
10, 1719–1754, 2010

be paid to the role of downward mixing ozone or the ozone from the preceding day in the study of ozone pollution.

4 Summary

This study experimentally investigates complete evolutions of ozone reservoir layers in the coastal environment in Southern Taiwan. Very similar patterns of ozone reservoir layer evolutions are found in three consecutive nights. The daily evolution can be divided into two stages – from evening to midnight and from midnight to the next morning. In the first stage, a deepened ozone reservoir layer initially forms from just above the ground to an altitude of 1300 m. Then large decrease in ozone concentration occurs below 800 m from evening to midnight. As a result, a concentrated, elevated ozone reservoir layer forms at 800–1200 m by midnight. In the second stage, the elevated ozone reservoir layer gradually descends, finally reaching 500–900 m in the next mid-morning. The evolutions of the observed ozone reservoir layers differ from the generally accepted evolution for an ozone reservoir layer, as presented in Fig. 1. The difference results from the fact that the general model was based on previous investigations performed in homogenous, inland environment, whereas the current observations were made in a coastal environment, where elevated transport is expected to be very complicated due to local circulations.

Comparisons between the variations in the observed ozone reservoir layers and the variations in wind field, potential temperature and water mixing ratio, as well as backward trajectory analyses, suggest that the observed ozone reservoir layers are formed by the invasion of cool, marine air masses into warmer, afternoon mixing layers. Elevated ozone reservoir layers are formed every midnight by the replacement of relatively clean marine air masses in the lower part of the initially formed ozone reservoir layers. Finally, nocturnal subsidence is responsible for the descending of the daily elevated ozone reservoir layers. The subsidence can enhance the ozone pollution in the following day because the ozone reservoir layers become lower and, therefore, are more

ACPD
10, 1719–1754, 2010

easily mixed into the growing mixing layer the next day. Additionally, since a sea-breeze circulation is much deeper than a land-breeze circulation, large point sources in a coastal region may significantly contribute to inland ozone pollution, because the plumes of coastal point sources can be transported inland in association with a landward, sea-breeze flow in the daytime and with a landward, returning land-breeze flow at night. This scenario is worthy of further study.

Based on observation-based methods, contributions of the downward mixing ozone and the ozone from the preceding day to the ozone accumulated on each of the four study days are examined. Usually, downward mixing ozone is expected to dominate daily at 08:00–10:00 LT when the surface inversion is broken. However, this work finds that a later, more important contribution is made at 11:00–12:00 LT, because the concentrated ozone reservoir layer is located at higher altitudes in a coastal environment than in an inland environment. This result reminds of the fact that the influence of downward mixing on surface ozone concentration is related to the vertical distribution of the ozone in an ozone reservoir layer. Furthermore, ozone distributions within the ozone reservoir layers are expected to be distributed far from being uniform, as presented in Fig. 1, particularly where local circulations dominate, as described in the current work. Finally, this work suggests that even in an area of high pollution and on a day of an ozone episode, downward mixing ozone or the ozone from the preceding day can still be 50% more important to daily ozone pollution than the ozone produced on the day of interest. Further understanding of ozone reservoir layers is critical and will rely upon the future simulation-based and experimental investigation.

Acknowledgements. The authors would like to thank the National Science Council (Contract No. NSC 95-2221-E-242-012) and the Environmental Protection Administration (EPA 95-FA11-03-D087) of the Republic of China, Taiwan, for financially supporting this research.

References

Akimoto, H., Mukai, H., Nishikawa, M., Murano, K., Hatakeyama, S., Liu, C. M., Buhr, M., Hsu, K. J., Jaffe, D. A., Zhang, L., Honrath, R., Merrill, J. T., and Newell, R. E.: Long-range transport of ozone in the East Asian Pacific rim region, J. Geophys. Res., 101, D1, 1999–2010, 1996.

Banta, R. M., Senff, C. J., White, A. B., Trainer, M., McNider, R. T., Valente, R. J., Mayor, S. D., Alvarez, R. J., Hardesty, R. M., Parrish, D., and Fehsenfeld, F. C.: Daytime buildup and nighttime transport of urban ozone in the boundary layer during a stagnation episode, J. Geophys. Res., 103, D17, 22519–22544, 1998.

Baumann, K., Williams, E. J., Angevine, W. M., Roberts, J. M., Norton, R. B., Frost, G. J., Fehsenfeld, F. C., Springston, S. R., Bertman, S. B., and Hartsell, B.: Ozone production and transport near Nashville, Tennessee: results from the 1994 study at New Hendersonville, J. Geophys. Res., 105, D7, 9137–9153, 2000.

Brown, S. S., Stark, H., Ryerson, T. B., Williams, E. J., Nicks Jr., D. K., Trainer, M., Fehsenfeld, F. C., and Ravishankara, A. R.: Nitrogen oxides in the nocturnal boundary layer: simultaneous in situ measurements of NO_3, N_2O_5, NO_2, NO, and O_3, J. Geophys. Res., 108, D9, 4299, doi:10.1029/2002JD002917, 2003.

Cantrell, C. A., Shetter, R. E., Gilpin, T. M., Calvert, J. G., Eisele, F. L., and Tanner, D. J.: Peroxy radical concentrations measured and calculated from trace gas measurements in the Mauna Loa Observatory Photochemistry Experiment 2, J. Geophys. Res., 101, D9, 14653–14664, 1996.

Cardelino, A. C. and Chameides, W. L.: The application of data from photochemical assessment monitoring stations to observation-based model, Atmos. Environ., 34, 2325–2332, 2000.

Chen, K. S., Ho, Y. T., Lai, C. H., and Chou, Y. M.: Photochemical modeling and analysis of meteorological parameters during ozone episodes in Kaohsiung, Taiwan, Atmos. Environ., 37, 1811–1823, 2003.

Cheng, W. L., Pai, J. L., Tsuang, B. J., and Chen, C. L.: Synoptic patterns in relation to ozone concentrations in west-central Taiwan, Meteorol. Atmos. Phys., 78, 11–21, 2001.

Dabberdt, W. F., Carroll, M. A., Baumgardner, D., Carmichael, G., Cohen, R., Dye, T., Ellis, J., Grell, G., Grimmond, S., Hanna, S., Irwin, J., Lamb, B., Madronich, S., McQueen, J., Meagher, J., Odman, T., Pleim, J., Schmid, H. P., and Westphal, D. L.: Meteorological re-

search needs for improved air quality forecasting – report of the 11th prospectus development team of the US Weather Research Program, B. Am. Meteorol. Soc., 85, 563–586, 2004.
Evans, M. J., Shallcross, D. E., Lawa, K. S., Wild, J. O. F., Simmonds, P. G., Spain, T. G., Berrisford, P., Methven, J., Lewis, A. C., McQuaid, J. B., Pilling, M. J., Bandy, B. J., Penkett, S. A., and Pyle, J. A.: Evaluation of a Lagrangian box model using field measurements from EASE (Eastern Atlantic Summer Experiment) 1996, Atmos. Environ., 34, 3843–3863, 2000.
Frost, G. J., Trainer, M., Allwine, G., Buhr, M. P., Calvert, J. G., Cantrell, C. A., Fehsenfeld, F. C., Goldan, P. D., Herwehe, J., Hübler, G., Kuster, W. C., Martin, R., McMillen, R. T., Montzka, S. A., Norton, R. B., Parrish, D. D., Ridley, B. A., Shetter, R. E., Walega, J. G., Watkins, B. A., and Westberg, H. H.: Photochemical ozone production in the rural southeastern United States during the 1990 Rural Oxidants in the Southern Environment (ROSE) program, J. Geophys. Res., 103, D17, 22491–22508, 1998.
Fuhrer, J.: Agroecosystem responses to combinations of elevated CO_2, ozone, and global climate change, Agr. Ecosyst. Environ., 97, 1–20, 2003.
Gerasopoulos, E., Kouvarakis, G., Vrekoussis, M., Donoussis, C., Mihalopoulos, N., and Kanakidou, M.: Photochemical ozone production in the Eastern Mediterranean, Atmos. Environ., 40, 3057–3069, 2006.
Hidy, G. M.: Ozone process insights from field experiments Part I: overview, Atmos. Environ., 34, 2001–2022, 2000.
Junker, C., Wang, J. L., and Lee, C. T.: Evaluation of the effect of long-range transport of air pollutants on coastal atmospheric monitoring sites in and around Taiwan, Atmos. Environ., 43, 3374–3384, 2009.
Kleinman, L. I.: Photochemical formation of peroxides in the boundary layer, J. Geophys. Res., 91, 10889–10904, 1986.
Komhyr, W. D.: Electrochemical concentration cells for gas analysis, Ann. Geophys., 25, 203–210, 1969, http://www.ann-geophys.net/25/203/1969/.
Komhyr, W. D., Barnes, R. A., Brothers, G. B., Lathrop, J. A., and Opperman, D. P.: Electrochemical concentration cell ozonesonde performance evaluation during STOIC 1989, J. Geophys. Res., 100, 9231–9244, 1995.
Lin, C.-H., Wu, Y.-L., Lai, C.-H., Lin, P.-H., Lai, H.-C., and Lin, P.-L.: Experimental investigation of ozone accumulation overnight during a wintertime ozone episode in South Taiwan, Atmos.

Environ., 38, 4267–4278, 2004.
Lin, C. Y., Wang, Z., Chou, C. C. K., Chang, C. C., and Liu, S. C.: A numerical study of an autumn high ozone episode over Southwestern Taiwan, Atmos. Environ., 41, 3684–3701, 2007.
Lu, R. and Turco, R. P.: Air pollutant transport in a coastal environment. II: Three-dimensional simulations over Los Angeles basin, Atmos. Environ., 29, 1499–1518, 1995.
McKendry, I. G. and Lundgren, J.: Tropospheric layering of ozone in regions of urbanized complex and/or coastal terrain: a review, Prog. Phys. Geog., 24, 329–354, 2000.
National Research Council: Rethinking the Ozone Problem in Urban and Regional Air Pollution, National Academy Press, Washington, District of Columbia, 1991.
Neu, U., Kunzle, T., and Wanner, H.: On the relation between ozone storage in the residual layer and daily variation in near-surface ozone concentration – a case study, Bound.-Lay. Meteorol., 69, 221–247, 1994.
Placet, M., Mann, C. O., Gilbert, R. O., and Niefer, M. J.: Emissions of ozone precursors from stationary sources: a critical review, Atmos. Environ., 34, 2183–2204, 2000.
Russell, A. and Dennis, R.: NARSTO critical review of photochemical models and modeling, Atmos. Environ., 34, 2283–2324, 2000.
Shiu, C. J., Liu, S. C., Chang, C. C., Chen, J. P., Chou, C. C. K., Lin, C. Y., and Young, C. Y.: Photochemical production of ozone and control strategy for Southern Taiwan, Atmos. Environ., 41, 9324–9340, 2007.
Simpson, J. E.: Sea Breeze and Local Winds, Cambridge University Press, UK., 1994.
Spirig, C., Neftel, A., Kleinman, L. I., and Hjorth, J.: NO_x versus VOC limitation of O_3 production in the Po valley: local and integrated view based on observations, J. Geophys. Res., 107, D22, 8191, doi:10.1029/2001JD000561, 2002.
Stull, R. B.: An Introduction to Boundary Layer Meteorology, Kluwer Academic, London, 1998.
Stutz, J., Alicke, B., Ackermann, R., Geyer, A., White, A., and Williams, E.: Vertical profiles of NO_3, N_2O_5, O_3, and NO_x in the nocturnal boundary layer: 1. Observations during the Texas Air Quality Study 2000, J. Geophys. Res., 109, D12306, doi:10.1029/2003JD004209, 2004.
Taiwan EPA: Air Quality Annual Report, 2006, Taiwan Environment Protection Administration, Taipei, Taiwan, 2007.
Trainer, M., Buhr, M. P., Curran, C. M., Fehsenfeld, F. C., Hsie, E. Y., Liu, S. C., Norton, R. B., Parrish, D. D., Williams, E. J., Gandrud, B. W., Ridley, B. A., Shetter, J. D., Allwine, E. J., and Westberg, H. H.: Observations and Modeling of the Reactive Nitrogen Photochemistry

at a Rural Site, J. Geophys. Res., 96, D2, 3045–3063, 1991.
Trainer, M., Parrish, D. D., Goldan, P. D., Roberts, J., and Fehsenfeld, F. C.: Review of observation-based analysis of the regional factors influencing ozone concentrations, Atmos. Environ., 34, 2045–2061, 2000.
Wesely, M. L. and Hicks, B. B.: A review of the current status of knowledge on dry deposition, Atmos. Environ., 34, 2261–2282, 2000.
Whiteman, C. D., Zhong, S., Bian, X., Fast, J. D., and Doran, J. C.: Boundary layer evolution and regional-scale diurnal circulations over the Mexican plateau, J. Geophys. Res., 105, D8, 10081–10102, 2000.
Zhang, J. and Rao, S. T.: On the role of vertical mixing in the temporal evolution of ground-level zone concentrations, J. Appl. Meteorol., 38, 1674–1691, 1999.

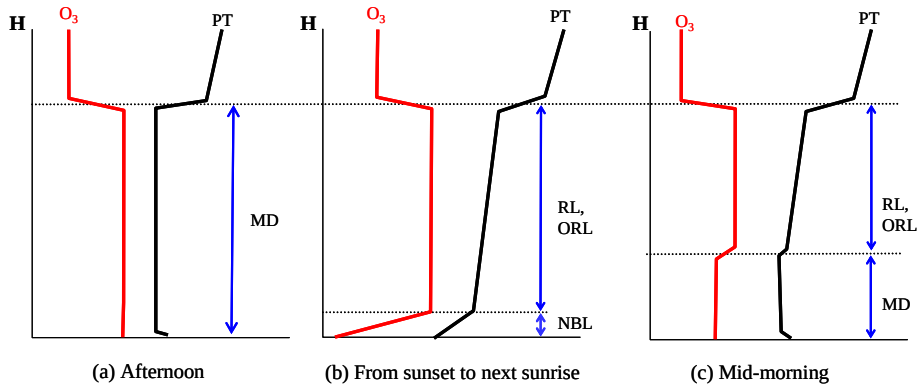

Fig. 1. Formation of ozone reservoir layer and its influence on surface ozone accumulation on the following day. **(a)** In the afternoon, ozone (O_3) is uniformly distributed in the convective mixing layer (MD), as revealed by the range of altitudes associated with a constant potential temperature (PT). **(b)** After sunset, surface cooling forms a nocturnal boundary layer (NBL), and the decay of turbulence within the previous mixing layer forms a residual layer (RL). The RL serves as an ozone reservoir layer (ORL) because ozone levels in this layer can remain as high as that in the previous mixing layer, due to a lack of ozone depleting sources, such as dry deposition and NO titration. **(c)** The following morning, the ozone in the RL or ORL can be mixed into the growing mixing layer and increasing the surface ozone levels.

ACPD
10, 1719–1754, 2010

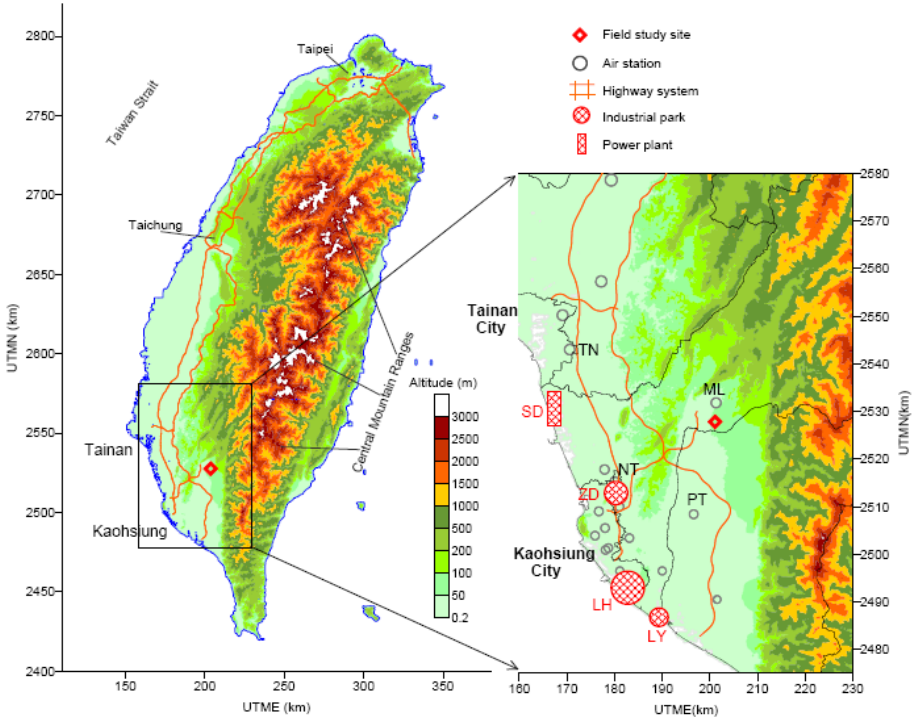

Fig. 2. Topography and location of field study site (diamond) and its surroundings, including air stations, highway systems, industrial parks and the most important power plant (SD) in Southern Taiwan.

ACPD
10, 1719–1754, 2010

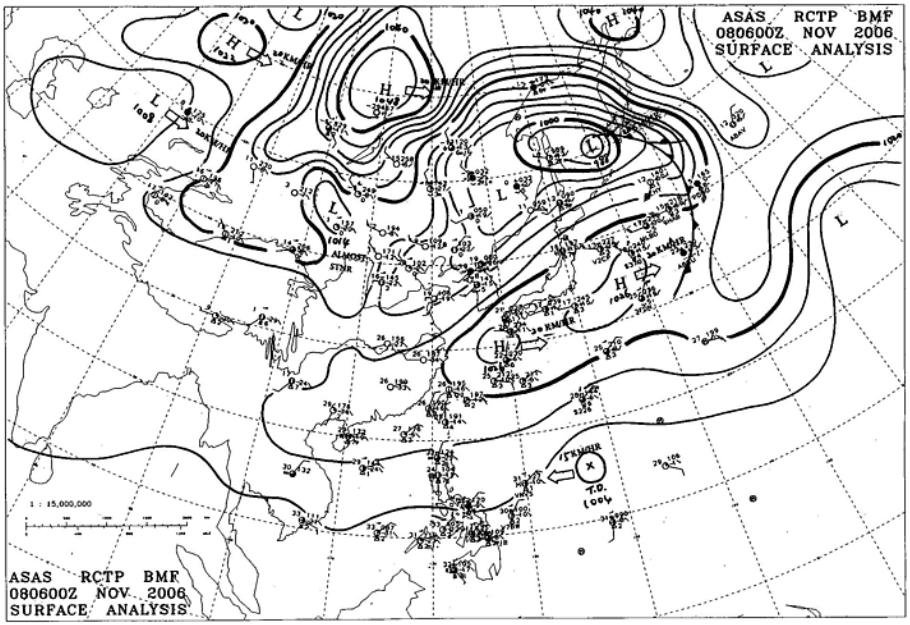

Fig. 3. Synoptic surface weather map on 8 November 2006 (Central Weather Bureau, Taiwan).

ACPD
10, 1719–1754, 2010

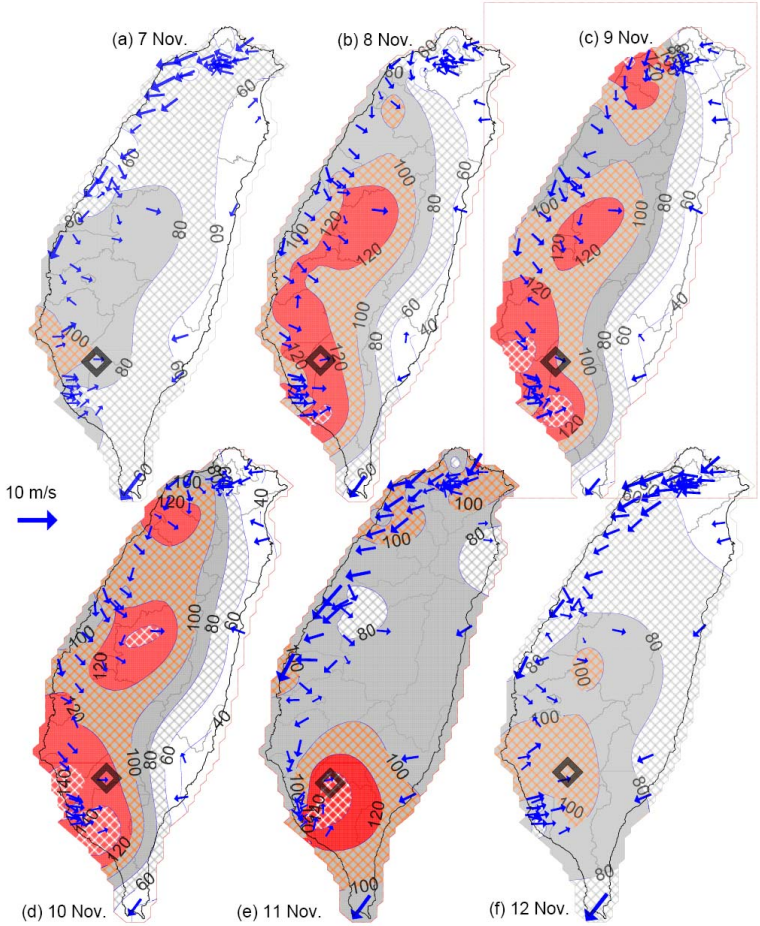

Fig. 4. Daily maximum hourly ozone contours and average wind fields at 12:00–16:00 LT throughout Taiwan, interpolated from the air stations of the Taiwan Air Quality Monitoring Network (TAQMN) during 7–12 November 2006. Diamonds represent the field study site.

ACPD
10, 1719–1754, 2010

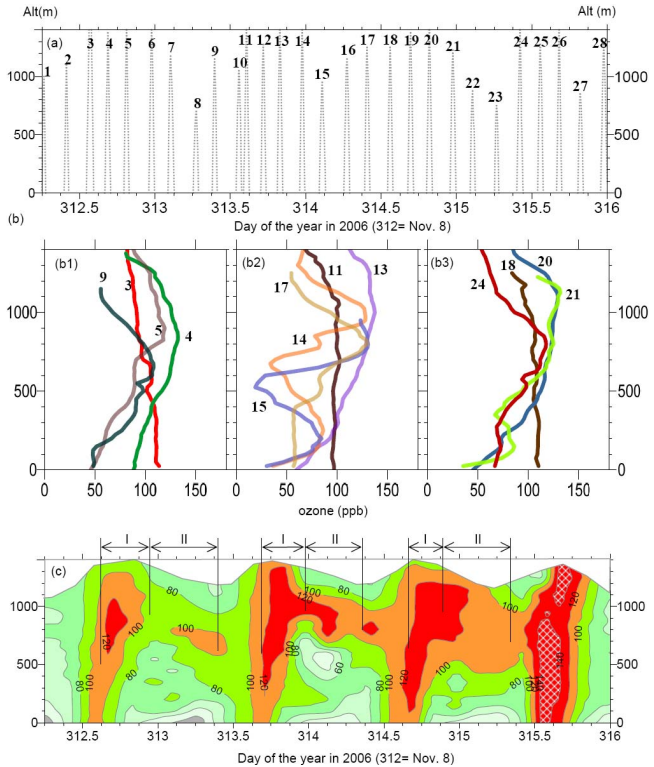

Fig. 5. (a) Time-height relationships of the ozone soundings and the number of soundings from 8 to 11 November 2006, **(b)** selected ozone profiles associated with numbers of soundings given in **(a)**, and **(c)** temporal evolution of vertical ozone distributions, produced from linear interpolations of measured ozone profiles in **(a)**. Profiles in **(b)** are averages of ascending and descending measurements; some upper parts of the ozone contours in **(c)** are blanked out to avoid false interpolations, due to lack of ozone measurement. Vertical thin lines in **(c)** represent stages I and II of daily ozone reservoir layer evolutions.

ACPD
10, 1719–1754, 2010

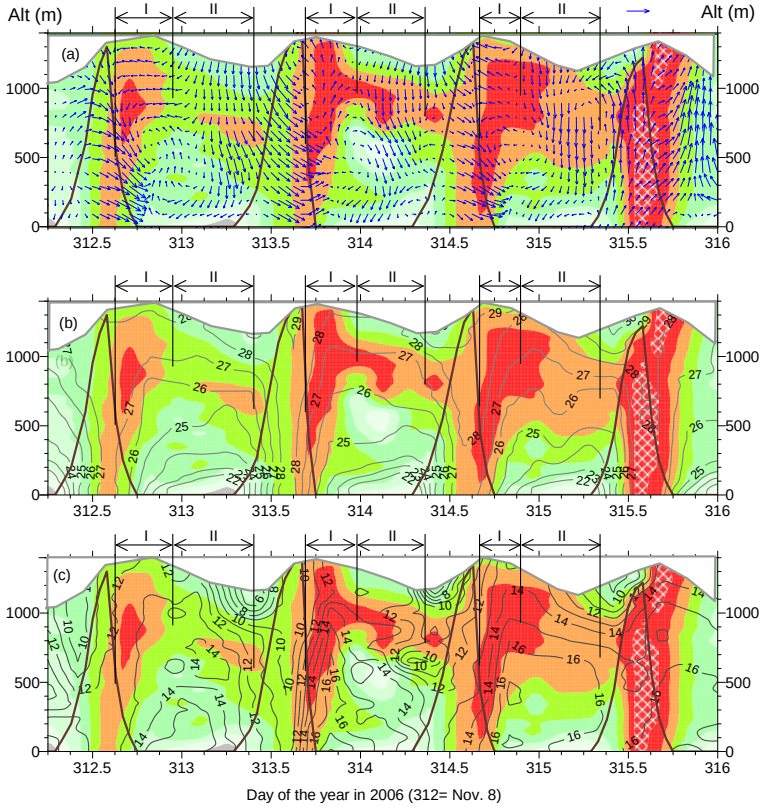

Fig. 6. As Fig. 5c, but for **(a)** winds, **(b)** potential temperature in Celsius, and **(c)** water mixing ratio in g/kg, superimposed on ozone contours (Fig. 5c). Solid thick lines represent convective mixing layers. Vertical thin lines represent stages I and II of daily ozone reservoir layer evolutions.

ACPD
10, 1719–1754, 2010

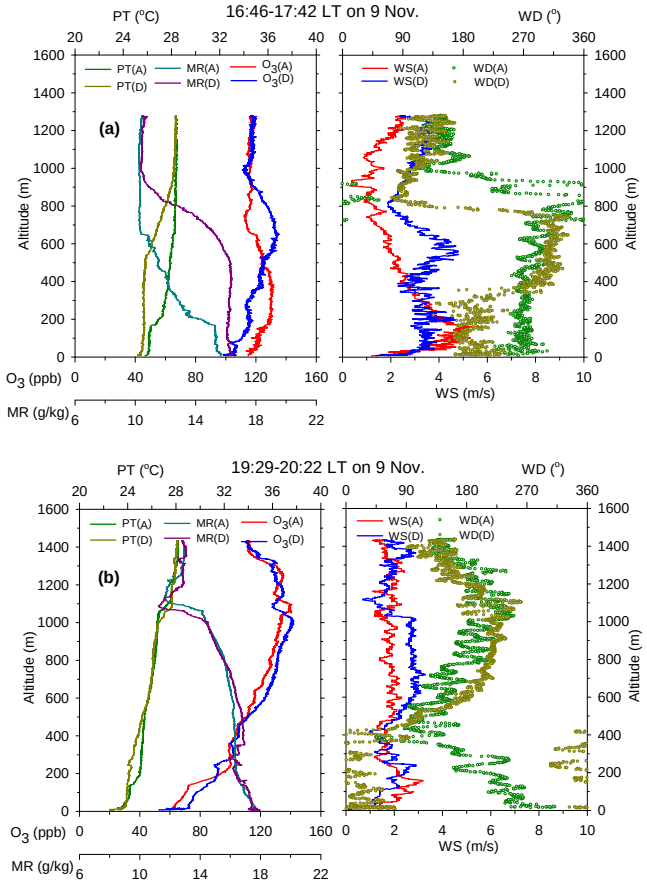

Fig. 7. Vertical profiles of ozone (O_3), potential temperature (PT), water mixing ratio (MR), wind speed (WS) and wind direction (WD), obtained from tethered soundings at study site at **(a)** 16:46–17:42 LT and **(b)** 19:29–20:22 LT on 9 November 2006. A and D represent ascending and descending measurements.

ACPD
10, 1719–1754, 2010

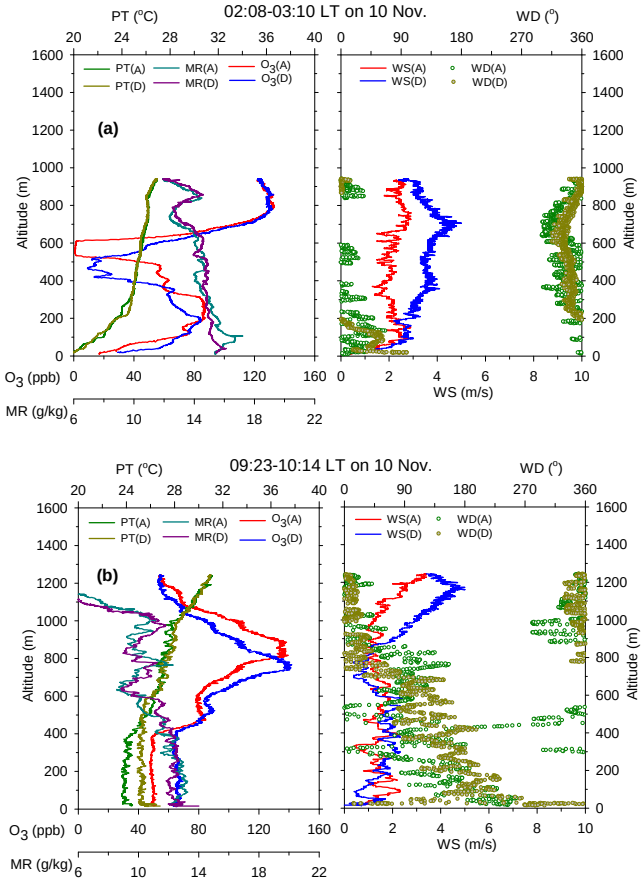

Fig. 8. As Fig. 7, but at **(a)** 02:08–03:10 LT and **(b)** 09:23–10:14 LT on 10 November 2006.

ACPD
10, 1719–1754, 2010

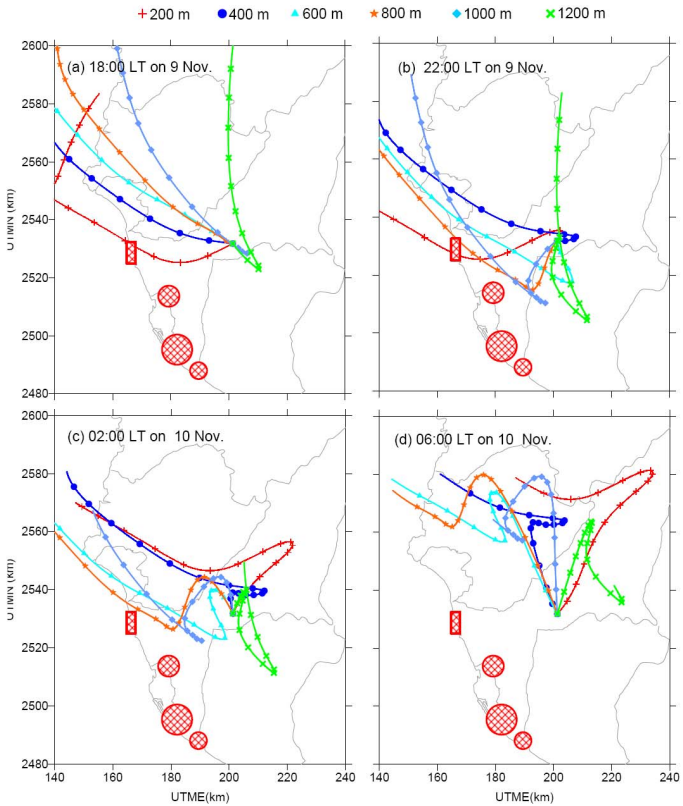

Fig. 9. Back air trajectories at 200, 400, 600, 800, 1000 and 1200 m, starting at study site at **(a)** 18:00 and **(b)** 22:00 LT on 9 November, **(c)** 02:00 and **(d)** 06:00 LT on 10 November. Distance between adjacent symbols in each trajectory represents one hour; circles and rectangular region indicate locations of industrial parks and SD power plant in Southern Taiwan, respectively (Fig. 2).

ACPD
10, 1719–1754, 2010

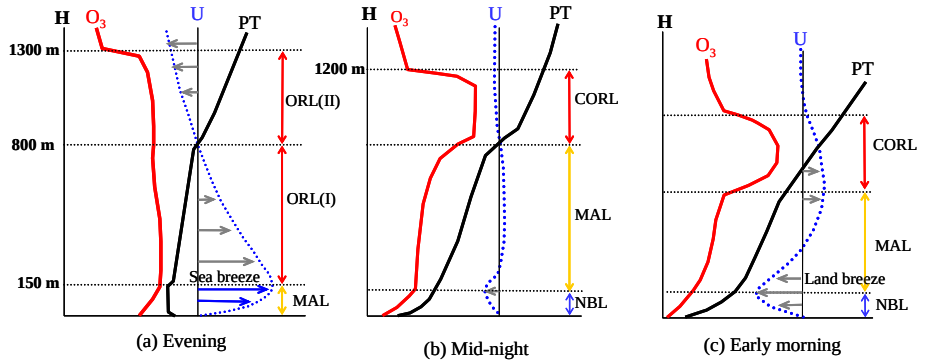

Fig. 10. General evolutions of vertical ozone distribution (O_3), wind (U) and potential temperature (PT) from evening to following morning at the studied coastal site. In the evening, **(a)** a sea-breeze circulation develops and an ozone reservoir layer is forms at 150–1300 m by the invasion of a cooler, marine air mass into a previous warmer, inland mixing layer. At this moment, the air layer below 150 m, MAL, is filled with marine air masses. The lower part of the ozone reservoir layer at 150–800 m, ORL(I), is a sea-breeze-like layer. However, it is filled with land-originated air masses. The upper part of the ozone reservoir layer at 800–1300 m, ORL(II), is a return-flow layer that is filled with inland-originated air masses. The sea-breeze circulation stops by midnight when **(b)** a concentrated, elevated ozone reservoir layer, CORL, forms at 800–1200 m, and is filled with inland-originated air masses. The air layer in the previous ORL(I) now is now filled with recently arrived, less polluted marine air masses, MAL. Additionally, a stable nocturnal boundary layer (NBL) is formed by surface cooling. From midnight to the following morning **(c)**, a land-breeze circulation develops. The CORL gradually descends and the previous MAR becomes shallow, due to nocturnal subsidence.

ACPD
10, 1719–1754, 2010

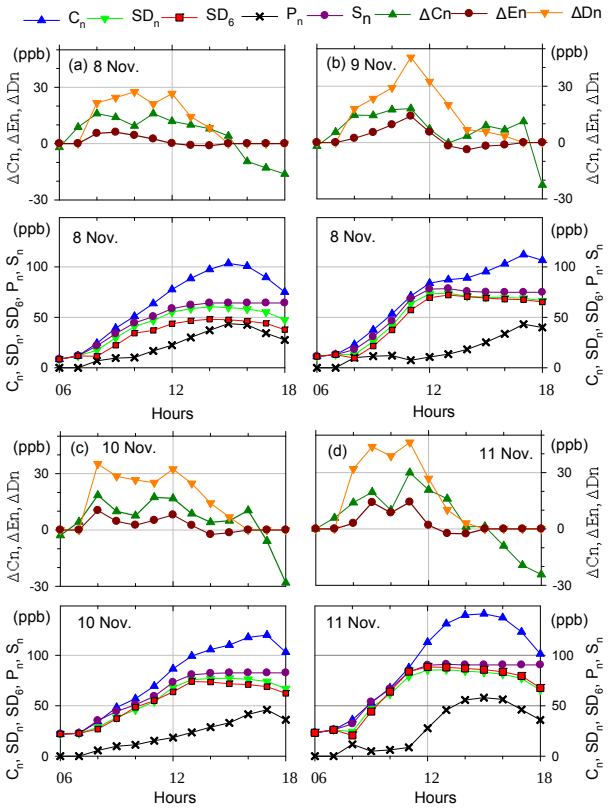

Fig. 11. Hourly variations of averaged ozone concentrations in the mixing layer (C_n), ozone concentrations from the preceding day with and without considering the dry deposition losses (SD_n and S_n), ozone contribution from the preceding day based on daily 06:00 LT ozone profiles (SD_6), ozone concentrations produced today (P_n), increase in ozone concentration in mixing layer (ΔC_n), downward mixing ozone concentration (ΔD_n), and net vertical entrainment ozone concentration (ΔE_n) on **(a)** 8, **(b)** 9, **(c)** 10, and **(d)** 11 November 2006.

ACPD
10, 1719–1754, 2010